Vibrations of rotors partially filled with liquids in hydrodynamically lubricated journal bearings

Dominik Kern [1], **Benedikt Wiegert**[2], **Michael Groß**[3]

[1] Institute for Applied Mechanics and Dynamics, TU Chemnitz, 09126 Chemnitz, Germany, dominik.kern@mb.tu-chemnitz.de
[2] Alumnus of Institute for Dynamics and Mechatronics, Karlsruhe Institute of Technology, 76049 Karlsruhe, Germany, benedikt.wiegert@alumni.kit.edu
[3] Institute for Applied Mechanics and Dynamics, TU Chemnitz, 09126 Chemnitz, Germany, michael.gross@mb.tu-chemnitz.de

Abstract

Rotors partially filled with liquid form an important subclass of rotating machinery. The liquid may either be part of the main functionality, e.g. in centrifuges and washing machines, or fulfill an auxiliary function such as cooling in motors and turbines. Many of these rotors run in hydrodynamically lubricated journal bearings. Both, the liquid filling as well as the liquid film in journal bearings, may cause self-excited oscillations. The latter leads to the well known oil-whirl and oil-whip instabilities, whereas the former may not only lead to instabilities but also to synchronization and balancing effects. This paper unites both branches of development and is guided by the questions: how do these effects influence each other, and how can stabilizing effects be reached, if they exist. Therefore, the classical planar model of a Laval-rotor with circular cross section, symmetry w.r.t. the middle plane (axial direction), imbalance and running at a prescribed rotational speed is modified. It is combined with reduced models for the bearings and the liquid filling. The bearing forces are calculated by Reynolds equation under the simplifying assumption for short bearings. The liquid filling is reduced to a rigid body, which interacts via discrete springs and dash-pots with the rotor. The liquid-filled rotor-bearing-system is studied by a run-up simulation and a bifurcation analysis.

1 Introduction

A washing machine is an illustrative example of a rotor which is partially filled with liquid. In industry, this type of rotor can be found in centrifuges as well as in some motors and turbines with hollow shafts for coolants. Like many rotors, they often run in hydrodynamically lubricated journal bearings. This paper tries to unify both, the liquid filling inside the rotor and the liquid film in the journal bearings, in one model. Up to now both branches were studied separately.

The investigation of liquid-film bearings is a fundamental issue in machines and mechanisms. Consequently it has a long history. The theoretical foundations were provided by Reynolds (Reynolds, 1886), who simplified the Navier-Stokes equations w.r.t. the conditions in a thin liquid layer as it occurs in journal bearings. The effects of oil-whirl and oil-whip instabilities have been experimentally observed by Newkirk & Taylor (Newkirk and Taylor, 1925) and later on exhaustively studied by many authors (Stodola, 1925; Hummel, 1926; Hori, 1959; Lund, 1966; Shaw and Shaw, 1990). The starting point in this paper is the work of Moser (Moser, 1993), in which rigid rotors in journal bearings and the resulting self-excited vibrations are considered.

The influence of liquids in cavities of rigid bodies goes back to Stokes (Stokes, 1847). It received much attention in the development of missiles and spacecrafts, whose main results are collected in the monograph by Moiseyev & Rumyantsev (Moiseyev and Rumyantsev, 2012). The technical relevance for rotors was experimentally revealed by Kollmann (Kollmann, 1962) and later theoretically investigated by many authors (Hendricks and Morton, 1979; Brommundt and Ostermeyer, 1986; Daich and Bar, 1973; Berman, Lundgren and Cheng, 1985). Beside self-excited vibrations which cause instabilities, there are also stabilizing effects which are utilized by liquid balancers (Langthjem and Nakamura, 2014). The liquid is an infinite-dimensional system and may only be solved analytically for special cases. In general it needs to be discretized. The direct approach by Computational Fluid Dynamics (CFD) methods, such as finite differences, volumes or elements, is still computationally too expensive

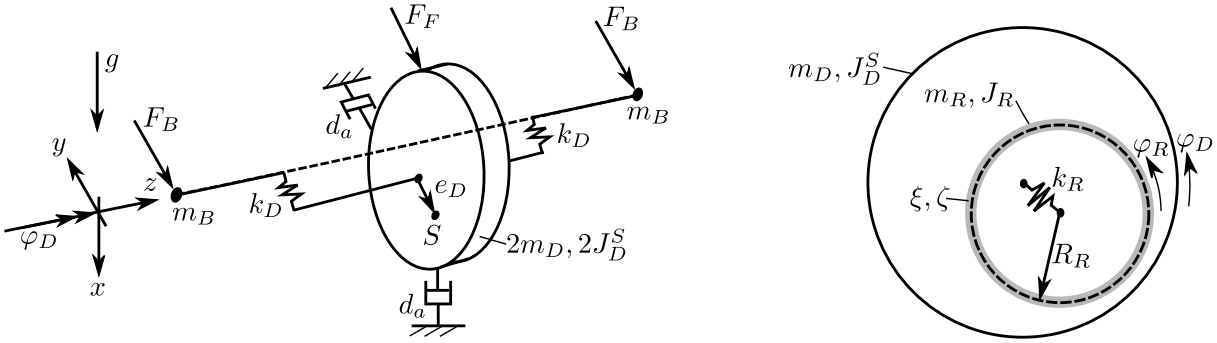

Figure 1: System model, left image: symmetric Laval-like-rotor model leading to a planar description; right image: the discrete model of the liquid filled rotor, where the liquid is reduced to a rigid ring (mass m_R) elastically connected (spring stiffness k_R) with the rotor center and sliding (friction coefficients ξ,ζ) over the rotor disk.

for repeated evaluations. The indirect approach by reduction of the liquid to an equivalent multi-body-system (Wolf, 1968; Lichtenberg, 1981) is of low dimension and allows to include the model in further studies, e.g. bifurcation analysis by numerical continuation. The most recent work about the reduction of a fluid continuum model to a multi-body system comes from Derendyaev et al. (Derendyaev, Vostrukhov and Soldatov, 2006), who developed a discrete model that matches the dynamics of the continuous system very well for a wide range of operation conditions, in which the liquid motion is dominated by a slow wave, i.e. one peak of the liquid surface. However, they prepared the model for taking ball bearings into account, but not for hydrodynamically lubricated journal bearings. It is worth mentioning that this reduced model shares some common features with the models used for automatic rotor balancing.

The composition of the model leading to the equation of motion is explained next in section 2 and followed by numerical results for an example system in section 3.

2 Modelling

The model is composed of three submodels. Firstly, the structural part of the rotor, which is reduced to rigid bodies and discrete springs. Secondly, the liquid-film bearings, which are modelled as nonlinear force elements. And thirdly, the liquid filling which is reduced to a rigid body, which interacts with the rotor via a spring and a complex viscous friction law. The rotor system is assumed to be symmetric w.r.t. the middle plane (axial direction). Furthermore the motion shall be dominated by the rotation around the rotor axis, thus a planar description suffices to account for the salient effects.

2.1 Rotor Model

The structural part is modelled similarly to the classical Laval-rotor (Gasch, Nordmann and Pfützner, 2006). As illustrated in fig. 1 (left), the inertia of the rotor is concentrated in one disk with mass $2m_D$ and mass moment of inertia $2J_D^S$. Its elasticity is represented by massless springs k_D between disk and bearings. The rotor axis is parallel to a principal axis of inertia, but not necessarily passing through the center of gravity, thus there may by an imbalance specified by the distance e_D. Further it is assumed that the disk rotates only around the z-axis with angular velocity $\dot{\varphi}_D$, but not around the x- and y-axes, i.e. no gyroscopic effects occur. In extension to the Laval-rotor additional point masses m_B are introduced in the bearings in order to account for the dynamics between rotor and the liquid films in the bearings. Furthermore, the rotor is aligned horizontally and subjected to gravity. Its equations of motion for one half (axial symmetry) read

$$m_B\ddot{x}_B + k_D(x_B - x_D) = F_{Bx}(x_B, \dot{x}_B, y_B, \dot{y}_B) + m_B g \tag{1a}$$
$$m_B\ddot{y}_B + k_D(y_B - y_D) = F_{By}(x_B, \dot{x}_B, y_B, \dot{y}_B) \tag{1b}$$
$$m_D\ddot{x}_D + d_a\dot{x}_D + k_D(x_D - x_B) = F_{Fx}(x_D, \dot{x}_D, y_D, \dot{y}_D, \dot{\varphi}_D) + m_D\big(e_D(\dot{\varphi}_D^2\cos\varphi_D + \ddot{\varphi}_D\sin\varphi_D) + g\big) \tag{1c}$$
$$m_D\ddot{y}_D + d_a\dot{y}_D + k_D(y_D - y_B) = F_{Fy}(x_D, \dot{x}_D, y_D, \dot{y}_D, \dot{\varphi}_D) + m_D e_D(\dot{\varphi}_D^2\sin\varphi_D - \ddot{\varphi}_D\cos\varphi_D) \tag{1d}$$
$$J_D^S\ddot{\varphi}_D = M_D + e_D(k_D y_D + d_a\dot{y}_D)\cos\varphi_D - e_D(k_D x_D + d_a\dot{x}_D)\sin\varphi_D, \tag{1e}$$

where x_B, y_B, x_D and y_D are the coordinates of the rotor masses in the bearings and the disk, respectively. The spring k_D represents the rotor elasticity, the dash-pot d_a subsumes all dissipative effects, while the torque M_D drives the rotor. The bearing resultant force F_B and the liquid filling resultant force F_F are to be specified next.

2.2 Bearing Model

The bearing forces are the resultants of the liquid pressure acting on rotor and bearings. The derivation given here is a brief summary of Moser's thesis (Moser, 1993). An incompressible lubricant of constant viscosity with vanishing inertial and external forces compared to the viscous forces is assumed. The lubrication film obeys then a reduced Navier-Stokes equation and the continuity equation

$$\nabla p = \frac{\eta_B}{\varrho}\nabla^2 \mathbf{v}, \tag{2}$$

$$\nabla \cdot \mathbf{v} = 0. \tag{3}$$

where $\mathbf{v}$ denotes velocity, p pressure and ϱ density. Using polar coordinates r, φ, z and making further assumptions of

- a vanishing pressure gradient in radial direction $\frac{\partial p}{\partial r} \approx 0$,
- domination of lowest order terms in $\frac{1}{r}$ for the Laplacian,
- domination of the derivatives of the velocities w.r.t. radius $\frac{\partial v_i}{\partial r} \gg \frac{\partial v_i}{\partial z}$ with $i = r, \varphi, z$ and
- approximation of terms $1/r$ by $1/R_B$, where R_B denotes the bearing radius.

In consequence eqs. (2)-(3) simplify to Reynolds' equation (Szeri, 2005)

$$\frac{1}{R_B^2}\frac{\partial}{\partial \varphi}\left(\frac{h^3}{\eta_B}\frac{\partial p}{\partial z}\right) + \frac{\partial}{\partial z}\left(\frac{h^3}{\eta_B}\frac{\partial p}{\partial z}\right) = 12\frac{\partial h}{\partial t} + 6\omega\frac{\partial h}{\partial \varphi}, \tag{4}$$

with oil film height h and angular velocity ω of the rotor. This partial differential equation is the starting point for most works on rotors in liquid film bearings. The pressure p is the unknown to solve for, while the oil film height and its derivatives follow geometrically from the rotor's motion. In order to recognize the next simplification, Reynolds' equation (4) is made dimensionless by relating the dimensions to bearing gap C, bearing width B_B and angular velocity ω of the rotor

$$\bar{z} = \frac{2z}{B_B}, \qquad H = \frac{h}{C}, \qquad \tau = \omega t, \quad \Pi = \frac{C^2}{R_B^2}\frac{p}{\eta_B \omega}, \tag{5a}$$

$$\Rightarrow \qquad \frac{\partial}{\partial \varphi}\left(H^3\frac{\partial \Pi}{\partial \bar{z}}\right) + \left(\frac{2R_B}{B_B}\right)^2\frac{\partial}{\partial \bar{z}}\left(H^3\frac{\partial \Pi}{\partial \bar{z}}\right) = 12\frac{\partial H}{\partial \tau} + 6\frac{\partial H}{\partial \varphi}. \tag{5b}$$

Assuming short bearings ($B_B < R_B$) the second term on the left hand side dominates and thus the first term is neglected. Then it is possible to integrate for the pressure analytically, which is subjected to the boundary conditions of ambient pressure in axial direction

$$\Pi = \left(\frac{B_B}{2R_B}\right)^2\frac{3}{H^3}\left(\frac{\partial H}{\partial \varphi} + 2\frac{\partial H}{\partial \tau}\right)^2(\bar{z}^2 - 1). \tag{6}$$

The pressure depends on the oil film height which follows from the planar motion of a smaller circle (rotor) moving in a larger circle (bearings). To evaluate the pressure, the following derivatives of the oil film height are needed

$$\frac{\partial H}{\partial \varphi} = \epsilon \sin(\varphi - \gamma), \tag{7a}$$

$$\frac{\partial H}{\partial \tau} = -\frac{\partial \epsilon}{\partial \tau}\cos(\varphi - \gamma) - \epsilon\frac{\partial \gamma}{\partial \tau}\sin(\varphi - \gamma), \tag{7b}$$

where $\epsilon = e_B/C$ is the dimensionless eccentricity of the rotor in the bearings and γ the angle to the narrowest gap of the liquid film there. These variables e_B and γ can also be understood as polar coordinates of the rotor's center. The resulting oil film forces follow by integration over the bearings area

$$F_{Bx}(e_B, e'_B, \gamma, \gamma') = -R_B \int_{-B_B/2}^{B_B/2} \int_{\Phi_1}^{\Phi_2} p(\Phi, z, e_B, e'_B, \gamma, \gamma') \cos\Phi \, \mathrm{d}\Phi \mathrm{d}z, \tag{8a}$$

$$F_{By}(e_B, e'_B, \gamma, \gamma') = -R_B \int_{-B_B/2}^{B_B/2} \int_{\Phi_1}^{\Phi_2} p(\Phi, z, e_B, e'_B, \gamma, \gamma') \sin\Phi \, \mathrm{d}\Phi \mathrm{d}z. \tag{8b}$$

These integrals can be solved analytically (Sommerfeld, 1955). It is not reasonable to integrate the pressure along the full circumference ($\Phi = 0 \ldots 2\pi$), as it becomes negative in some segment. This is not physical, because this means the oil would "pull" the rotor. There exist several proposals to resolve this discrepancy, the one chosen here is to determine the integration limits by the Gümbel boundary condition (Gümbel and Everling, 1925) in circumferential direction which states that the pressure is nowhere negative, i.e. $\Pi(\Phi_1) = 0$, $\frac{\partial \Pi}{\partial \Phi}\big|_{\Phi=\Phi_1} > 0$ and $\Pi(\Phi_2) = 0$, $\frac{\partial \Pi}{\partial \Phi}\big|_{\Phi=\Phi_2} < 0$. Finally, the bearing forces are determined as functions of the rotor position and angular velocity.

2.3 Liquid Filling Model

Liquids are naturally described as a continuum. This description we call "'continuous model"' of the liquid filling inside the rotor. However, this work uses a reduction of the liquid to an equivalent rigid body in order to reduce the problem complexity. This latter description we refer to as "'discrete model"'. The model reduction for a liquid partially filling a cylindrical cavity (coaxial) is adopted from Derendyaev et al. (Derendyaev et al., 2006). They reduce the liquid to a ring-shaped rigid body, which is elastically connected to the rotor's center and subjected to a complex friction law, as shown in fig. 1 (right). Its mass and moment of inertia represent the density of the liquid, the elastic spring the force field action and the friction law the viscosity (liquid entrainment). While mass and spring are well-known discrete elements, the friction law is sort of unusual, it reads for the distributed friction force along the contact line between disk and ring

$$\mathbf{f}_\eta = -\xi(\mathbf{v}_R - \mathbf{v}_D) - \zeta \mathbf{e}_z \times (\mathbf{v}_R - \mathbf{v}_D). \tag{9}$$

At the first glance this seems like a typical linear viscous friction law, since the force is proportional to the relative velocity between ring (liquid) and disk (rotor). However, this friction force is not collinear to the relative velocity. This peculiarity seems strange from a rigid-body-dynamics point of view. The perpendicular component will be further referred to as *gyroscopic*, although it does not depend on the angular velocity. It may be related to Coriolis effects in the boundary layer, however its best justification is the good agreement achievable between discrete and continuous model. The resulting friction force follows from integration along the contact line which is a circle of radius R_R and circumference $L = 2\pi R_R$. It contributes to the interaction force between rotor and liquid filling

$$F_{Fx} = -k_R(x_R - x_D) - \xi L\big((\dot{x}_R - \dot{x}_D) + (y_R - y_D)\dot{\varphi}_D\big) + \zeta L\big((\dot{y}_R - \dot{y}_D) - (x_R - x_D)\dot{\varphi}_D\big), \tag{10a}$$

$$F_{Fy} = -k_R(y_R - y_D) - \xi L\big((\dot{y}_R - \dot{y}_D) - (x_R - x_D)\dot{\varphi}_D\big) - \zeta L\big((\dot{x}_R - \dot{x}_D) + (y_R - y_D)\dot{\varphi}_D\big). \tag{10b}$$

So far only the parameters of the continuous model: viscosity η_F, mass m_F, and filling ratio δ_F (liquids inner radius to outer radius) are known. The conversion to the discrete model (ring mass m_R, ring radius R_R, spring stiffness k_R, viscous friction parameters ξ, ζ) is done by matching of the stability limits, i.e. the discrete parameters are tuned such that the stability domains of the discrete model coincide well with the stability domains of the continuous model. This works well for the slow wave mode and sufficiently for the fast wave mode. This procedure is only feasible for the balanced rotor without external force fields, such as gravitation, because it relies on analytical solutions of the continuous model. Beyond these assumptions, the reduced model is supposed to approximate the liquid sufficiently accurate. The obtained discrete model has three degrees of freedom and reduces the computational cost drastically compared to the continuous model. Note, that the model is based on the assumption of a ring-shaped liquid distribution and thus its validity has limits. Firstly, the rotational velocity must be fast enough to maintain a circular liquid distribution. Secondly, the rotor accelerations, translational and rotational, are limited, as they should not excite higher wave modes.

2.4 Equation of Motion

Combining all three subsystems leads to equations of motion of MDGKZ-type

$$\mathbf{M}\ddot{\mathbf{x}} + (\mathbf{D}+\mathbf{G})\dot{\mathbf{x}} + (\mathbf{K}+\mathbf{Z})\mathbf{x} = \mathbf{f}(t,\mathbf{x},\dot{\mathbf{x}}), \tag{11a}$$

$$J_R\ddot{\varphi}_R + \xi L R_R^2 \dot{\varphi}_R = \xi L R_R^2 \dot{\varphi}_D(t), \tag{11b}$$

where the vector $\mathbf{x} = [x_B, y_B, x_D, y_D, x_R, y_R]^T$ contains the positions of rotor-bearings, rotor-disk and liquid-ring. These equations are written separately for the translational motion and for the rotation in order to emphasize the fact, that there is no coupling between them, if the rotor angle is not a degree of freedom. This assumption of a prescribed rotational velocity $\dot{\varphi}_D = \omega(t)$ holds for the remainder of this paper. The matrices of mass $\mathbf{M}$, damping $\mathbf{D}$, gyroscopic terms $\mathbf{G}$, stiffness $\mathbf{K}$, circulatoric terms $\mathbf{Z}$ and right hand side $\mathbf{f}$ are given by

$$\mathbf{f} = \begin{bmatrix} F_{Bx}(x_B,\dot{x}_B,y_B,\dot{y}_B) + m_B g \\ F_{By}(x_B,\dot{x}_B,y_B,\dot{y}_B) \\ m_D e_D(\dot{\varphi}_D^2\cos\varphi_D + \ddot{\varphi}_D\sin\varphi_D) + m_D g \\ m_D e_D(\dot{\varphi}_D^2\sin\varphi_D - \ddot{\varphi}_D\cos\varphi_D) \\ m_R g \\ 0 \end{bmatrix}, \qquad \mathbf{M} = \begin{bmatrix} m_B & 0 & 0 & 0 & 0 & 0 \\ 0 & m_B & 0 & 0 & 0 & 0 \\ 0 & 0 & m_D & 0 & 0 & 0 \\ 0 & 0 & 0 & m_D & 0 & 0 \\ 0 & 0 & 0 & 0 & m_R & 0 \\ 0 & 0 & 0 & 0 & 0 & m_R \end{bmatrix}, \tag{12}$$

$$\mathbf{D} = \begin{bmatrix} 0 & 0 & 0 & 0 & 0 & 0 \\ 0 & 0 & 0 & 0 & 0 & 0 \\ 0 & 0 & d_a+d_\xi & 0 & -d_\xi & 0 \\ 0 & 0 & 0 & d_a+d_\xi & 0 & -d_\xi \\ 0 & 0 & -d_\xi & 0 & d_\xi & 0 \\ 0 & 0 & 0 & -d_\xi & 0 & d_\xi \end{bmatrix}, \qquad \mathbf{G} = \begin{bmatrix} 0 & 0 & 0 & 0 & 0 & 0 \\ 0 & 0 & 0 & 0 & 0 & 0 \\ 0 & 0 & 0 & -d_\zeta & 0 & d_\zeta \\ 0 & 0 & d_\zeta & 0 & -d_\zeta & 0 \\ 0 & 0 & 0 & d_\zeta & 0 & -d_\zeta \\ 0 & 0 & -d_\zeta & 0 & d_\zeta & 0 \end{bmatrix}, \tag{13}$$

$$\mathbf{K} = \begin{bmatrix} k_D & 0 & -k_D & 0 & 0 & 0 \\ 0 & k_D & 0 & -k_D & 0 & 0 \\ -k_D & 0 & k_D+\tilde{k} & 0 & -\tilde{k} & 0 \\ 0 & -k_D & 0 & k_D+\tilde{k} & 0 & -\tilde{k} \\ 0 & 0 & -\tilde{k} & 0 & \tilde{k} & 0 \\ 0 & 0 & 0 & -\tilde{k} & 0 & \tilde{k} \end{bmatrix}, \qquad \mathbf{Z} = \begin{bmatrix} 0 & 0 & 0 & 0 & 0 & 0 \\ 0 & 0 & 0 & 0 & 0 & 0 \\ 0 & 0 & 0 & d_\xi\dot{\varphi}_D & 0 & -d_\xi\dot{\varphi}_D \\ 0 & 0 & -d_\xi\dot{\varphi}_D & 0 & d_\xi\dot{\varphi}_D & 0 \\ 0 & 0 & 0 & -d_\xi\dot{\varphi}_D & 0 & d_\xi\dot{\varphi}_D \\ 0 & 0 & d_\xi\dot{\varphi}_D & 0 & -d_\xi\dot{\varphi}_D & 0 \end{bmatrix}, \tag{14}$$

with $\tilde{k} = k_R + \zeta L\dot{\varphi}_D$, $d_\xi = \xi L$ and $d_\zeta = \zeta L$. Note that the right hand side contains not only time dependent excitations, but also nonlinear terms of the bearing forces and the imbalance.

2.5 Dimensionless Equations

A dimensionless formulation reduces the number of parameters of the system and it leads to a compact description of the qualitative behaviour. The expressions for converting the equations of motion (11a)-(11b) into dimensionless form are summarized in table 1. For a rotor running with constant angular velocity $\dot{\varphi}_D(t) = \omega$, the dimensionless equations of motion read

$$\bar{\mathbf{M}}\bar{\omega}^2\bar{\mathbf{x}}'' + (\bar{\mathbf{D}}+\bar{\mathbf{G}})\bar{\omega}\bar{\mathbf{x}}' + (\bar{\mathbf{K}}_0 + \bar{\mathbf{K}}_1\bar{\omega})\bar{\mathbf{x}} = \bar{\mathbf{f}}(\tau,\bar{\mathbf{x}},\bar{\mathbf{x}}'), \tag{15a}$$

$$\bar{J}_R\bar{\omega}^2\bar{\varphi}_R'' + \bar{d}_R\bar{\omega}\bar{\varphi}_R' = \bar{d}_R\bar{\omega}, \tag{15b}$$

where instead of symmetric $\bar{\mathbf{K}}$ and skew-symmetric $\bar{\mathbf{Z}}$, the distinction between constant $\bar{\mathbf{K}}_0$ and product with angular velocity $\bar{\omega}\bar{\mathbf{K}}_1$ was made. The prime stands for differentiation w.r.t. dimensionless time $()' = \frac{\mathrm{d}}{\mathrm{d}\tau}()$. The

Table 1: Dimensionless coordinates and parameters

coordinates	$\bar{x}_i = \frac{x_i}{C}, \quad \bar{y}_i = \frac{y_i}{C}$	$i = B, D, R$
time	$\tau = \omega t$	$\omega = \dot{\varphi}_D,\ \varphi'_D = 1$
angular frequency	$\bar{\omega} = \omega\sqrt{C/g}$	
masses	$\bar{m}_i = \frac{m_i}{m}$	$i = B, D, R,\ m = m_L + m_D(+m_R)$
damping/friction	$\bar{d}_i = \frac{d_i}{m}\sqrt{\frac{C}{g}}$	$i = a, \xi, \zeta$
stiffnesses	$\bar{k}_i = \frac{C}{mg}k_i$	$i = D, R$
imbalance	$\rho = \frac{e_D}{C}$	
modified Sommerfeld number	$S_m = (\frac{R_B}{C})^2 \frac{2\eta_B \omega B_B R_B}{mg}(\frac{B_B}{2R_B})^2$	
reciprocal load parameter	$\sigma = \frac{S_m}{\bar{\omega}} = \frac{1}{2}\frac{R_B B_B^3 \eta_B}{C^2 m\sqrt{Cg}}$	$\sigma \to \infty$ means unloaded
moment of inertia	$\bar{J}_R = \frac{J_R}{mR_R C}$	
rotational damping	$\bar{d}_R = \frac{\xi L R_R}{m\sqrt{Cg}}$	

matrices of eq. (15a) are given by

$$\mathbf{f} = \begin{bmatrix} S_m f_x(\bar{x}_B, \bar{x}'_B, \bar{y}_B, \bar{y}'_B) + \bar{m}_B \\ S_m f_y(\bar{x}_B, \bar{x}'_B, \bar{y}_B, \bar{y}'_B) \\ \bar{m}_D \rho \bar{\omega}^2 \cos\tau + \bar{m}_D \\ \bar{m}_D \rho \bar{\omega}^2 \sin\tau \\ \bar{m}_R \\ 0 \end{bmatrix}, \qquad \mathbf{M} = \begin{bmatrix} \bar{m}_B & 0 & 0 & 0 & 0 & 0 \\ 0 & \bar{m}_B & 0 & 0 & 0 & 0 \\ 0 & 0 & \bar{m}_D & 0 & 0 & 0 \\ 0 & 0 & 0 & \bar{m}_D & 0 & 0 \\ 0 & 0 & 0 & 0 & \bar{m}_R & 0 \\ 0 & 0 & 0 & 0 & 0 & \bar{m}_R \end{bmatrix}, \tag{16}$$

$$\bar{\mathbf{D}} + \bar{\mathbf{G}} = \begin{bmatrix} 0 & 0 & 0 & 0 & 0 & 0 \\ 0 & 0 & 0 & 0 & 0 & 0 \\ 0 & 0 & \bar{d}_a + \bar{d}_\xi & 0 & -\bar{d}_\xi & 0 \\ 0 & 0 & 0 & \bar{d}_a + \bar{d}_\xi & 0 & -\bar{d}_\xi \\ 0 & 0 & -\bar{d}_\xi & 0 & \bar{d}_\xi & 0 \\ 0 & 0 & 0 & -\bar{d}_\xi & 0 & \bar{d}_\xi \end{bmatrix} + \begin{bmatrix} 0 & 0 & 0 & 0 & 0 & 0 \\ 0 & 0 & 0 & 0 & 0 & 0 \\ 0 & 0 & 0 & -\bar{d}_\zeta & 0 & \bar{d}_\zeta \\ 0 & 0 & \bar{d}_\zeta & 0 & -\bar{d}_\zeta & 0 \\ 0 & 0 & 0 & \bar{d}_\zeta & 0 & -\bar{d}_\zeta \\ 0 & 0 & -\bar{d}_\zeta & 0 & \bar{d}_\zeta & 0 \end{bmatrix}, \tag{17}$$

$$\bar{\mathbf{K}}_\mathbf{0} + \bar{\mathbf{K}}_1\bar{\omega} = \begin{bmatrix} \bar{k}_D & 0 & -\bar{k}_D & 0 & 0 & 0 \\ 0 & \bar{k}_D & 0 & -\bar{k}_D & 0 & 0 \\ -\bar{k}_D & 0 & \bar{k}_D + \bar{k}_R & 0 & -\bar{k}_R & 0 \\ 0 & -\bar{k}_D & 0 & \bar{k}_D + \bar{k}_R & 0 & -\bar{k}_R \\ 0 & 0 & -\bar{k}_R & 0 & \bar{k}_R & 0 \\ 0 & 0 & 0 & -\bar{k}_R & 0 & \bar{k}_R \end{bmatrix} + \begin{bmatrix} 0 & 0 & 0 & 0 & 0 & 0 \\ 0 & 0 & 0 & 0 & 0 & 0 \\ 0 & 0 & \bar{d}_\zeta & \bar{d}_\xi & -\bar{d}_\zeta & -\bar{d}_\xi \\ 0 & 0 & -\bar{d}_\xi & \bar{d}_\zeta & \bar{d}_\xi & -\bar{d}_\zeta \\ 0 & 0 & -\bar{d}_\zeta & -\bar{d}_\xi & \bar{d}_\zeta & \bar{d}_\xi \\ 0 & 0 & \bar{d}_\xi & -\bar{d}_\zeta & -\bar{d}_\xi & \bar{d}_\zeta \end{bmatrix} \bar{\omega}. \tag{18}$$

3 Numerical Results

There are three models under consideration, the empty rotor, the filled rotor and the equivalent-mass rotor. The filled rotor is heavier than the empty rotor, due to the added liquid. In order to differentiate between the effects of the added mass and the liquid there is the third model, which is an empty rotor but of the same mass as the filled one. Two kinds of study are performed a run-up simulation and a bifurcation analysis. The values of the model parameters are listed in the appendix (tab. 2).

3.1 Transient Simulation

There is no static equilibrium ($\ddot{\mathbf{x}} = \mathbf{0}$, $\dot{\mathbf{x}} = \mathbf{0}$) for a running rotor with imbalance, thus stationary periodic solutions are expected, which may become unstable with increasing rotational velocity. Although the model has

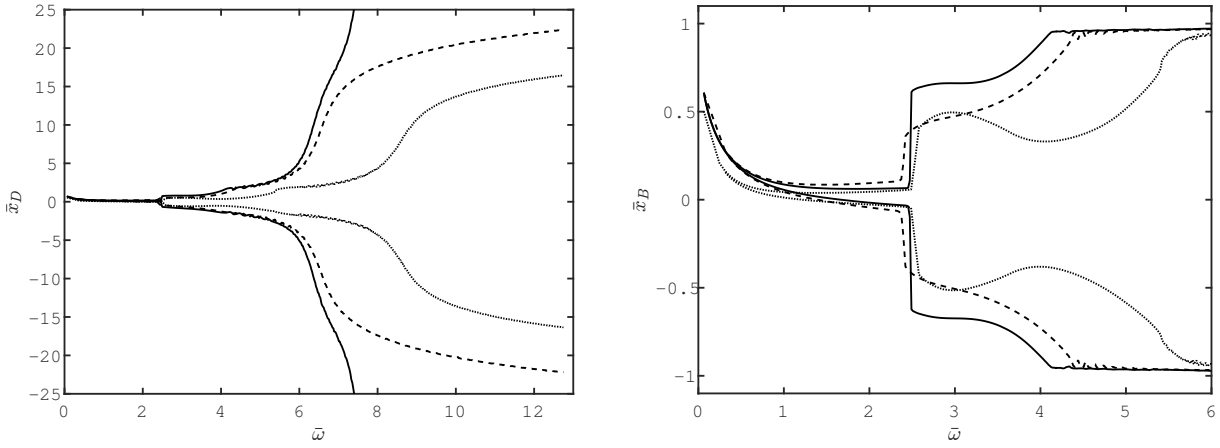

Figure 2: Envelope curves of the run-up simulation, left image: rotor disk position; right image: rotor position in the bearings for the empty rotor (dotted line), filled rotor (solid line) and equivalent-mass rotor (dashed line).

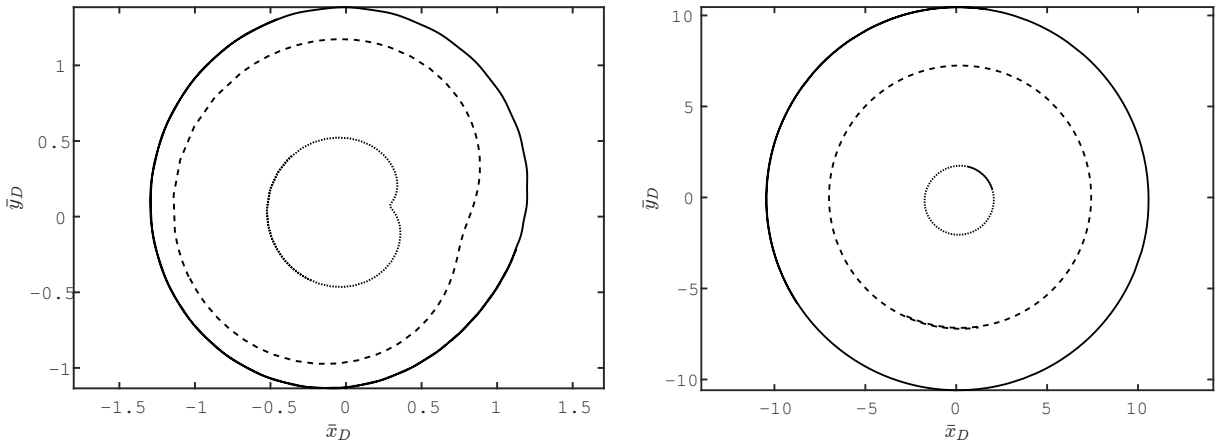

Figure 3: Trajectories of the rotor disk during the run-up simulation, left image: at $\bar{\omega} = 3.87$; right image: at $\bar{\omega} = 6.41$ for the empty rotor (dotted line), filled rotor (solid line) and equivalent-mass rotor (dashed line).

only seven/four degrees of freedom (with/without liquid filling), its transient simulation is time consuming. There are several time scales of motion requiring a solver for stiff ordinary differential equations. Here a variable-step, variable-order solver (MATLAB ode15s) based on numerical differentiation formulas (Shampine and Reichelt, 1997) has been applied. The run-up starts at $t = 0$ in the equilibrium position of the balanced rotor with a nonzero rotational velocity. Since the rotor is imbalanced, this causes some transient oscillations. The rotation frequency is linearly increased by

$$f_D(t) = 10\,\mathrm{Hz} + 20\frac{\mathrm{Hz}}{\mathrm{s}}t. \tag{19}$$

The initial rotational velocity was set in order to fulfill the condition $\omega > \sqrt{g/R_F}$, where R_F denotes the inner radius of the liquid in the rotationally symmetric state. This is at least necessary in order to maintain a circular liquid distribution which again is a prerequisite for the model order reduction of the liquid to an equivalent rigid body to be valid. In reality this transition from the liquid in the lower half to the ring-shaped distribution occurs at higher velocities, but for now these details are neglected. We assume that at a rotational speed slightly above the initial value the rotor arrives in a stable regime and the self-excited vibrations as well as further effects of interest occur at much higher frequencies.

In fig. 2 are classical results recognizable. The empty rotor starts with small periodic solutions. After 20s ($f_D = 410\,\mathrm{Hz}$, $\bar{\omega} = 2.6$) the amplitudes increase quickly due to oil-whirl. After further frequency increase at about 60s ($f_D = 1210\,\mathrm{Hz}$, $\bar{\omega} = 7.6$) the transition from oil-whirl to oil-whip begins, leading to high amplitudes

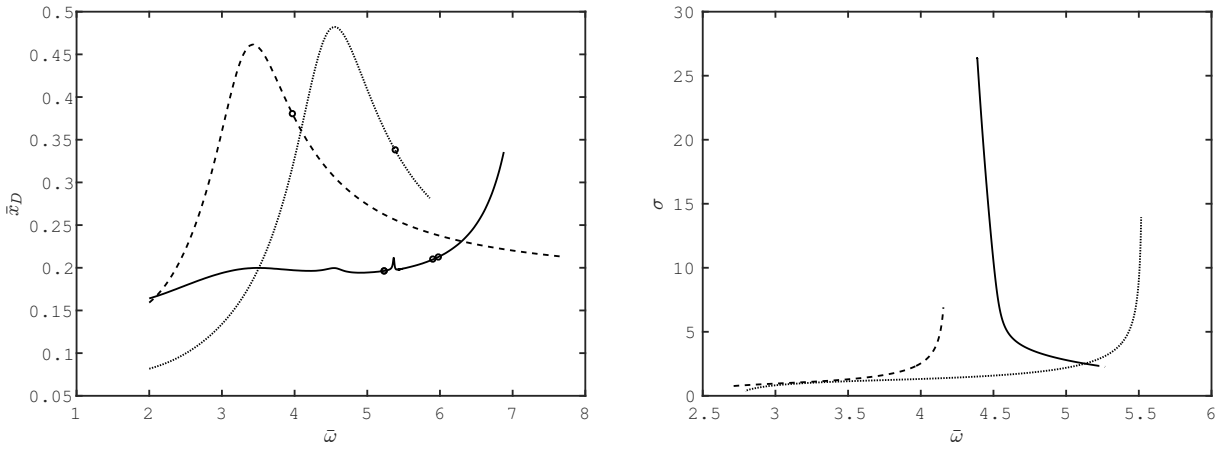

Figure 4: Bifurcation analysis, left image: dimensionless rotor angular velocity versus dimensionless rotor disk position, Neimark-Sacker bifurcations are denoted by circles; right image: path of the first Neimark-Sacker bifurcation in dependence on dimensionless angular velocity and dimensionless reciprocal load parameter for empty rotor (dotted line), filled rotor (solid line) and equivalent-mass rotor (dashed line).

where the rotor hits the bearings ($\sqrt{\bar{x}_B^2 + \bar{y}_B^2} = 1$). Beyond this point the model is not valid anymore, as this contact is not included. This is not relevant for practical applications anymore as such conditions are to be avoided anyway. The results beyond this point are only of theoretical interest. Fig. 3 shows two snapshots of the rotor disc trajectories during run-up, whose amplitudes increased by a factor of almost ten between $\bar{\omega} = 3.87$ and $\bar{\omega} = 6.41$.

The simulation with liquid filling coincides with the previous in the first 30s. Similarly, there is the onset of oil-whirl in the bearing after 20s, but then the envelope of the rotor disk oscillations diverges from the previous run until they begin to rise higher at about 40s ($f_D = 805\,\text{Hz}$, $\bar{\omega} = 5.1$) indicating a destructive mode of operation after 50s. At this point the effect of the liquid becomes apparent as its amplitude rise higher not only than those of the rotor of the emtpy rotor but also higher than those of the equivalent-mass rotor.

All three models start with stable periodic solutions. This confirms the assumption made initially about the begin of the run-up. For comparison are the eigenfrequencies given for the rotor only, i.e. when the bearings are assumed fixed

$$\begin{aligned} \bar{\omega}_e &= 4.52, \\ \bar{\omega}_{f1} &= 3.37, \qquad \bar{\omega}_{f2} = 17.58, \\ \bar{\omega}_{em} &= 3.41. \end{aligned}$$

These values correspond to the empty, filled and equilibrium-mass rotor, respectively.

3.2 Bifurcation Analysis

Firstly, the liquid-filled rotor-bearing-system is characterized by a bifurcation analysis w.r.t. the rotational speed. The remaining parameters keep their constant values. The stationary amplitudes of oscillations are logged by numerical continuation (Dhooge, Govaerts and Kuznetsov, 2003) and shown in fig. 4 (left). Beginning with limit cycles of small amplitude at a dimensionless frequency of $\bar{\omega} = 2$ there occurs a Neimark-Sacker bifurcation at $\bar{\omega} = 5.38$ for the empty rotor, i.e. from this point on there exist not only limit cycles but also torus oscillations (Kuznetsov, 2013). The filled rotor shows four Neimark-Sacker bifurcations in this range ($\bar{\omega} = 2 \ldots 7$), two very close at $\bar{\omega} = 5.23$ and the two others at $\bar{\omega} = 5.90$ and $\bar{\omega} = 5.98$. While the equivalent-mass rotor bifurcates earlier, at $\bar{\omega} = 3.97$.

Secondly, the first bifurcation point is tracked w.r.t. two parameters, the dimensionless frequency and reciprocal load parameter. Fig. 4 (right) shows the results, where the liquid filling leads to qualitative differences. Without liquid the dependence of the first bifurcation point is of positive slope in the $\bar{\omega}$-σ space, while for rotors filled with liquid it is of negative slope.

4 Summary

The analysis of liquid-filled rotors in hydrodynamically lubricated bearings was made feasible by reducing the infinite-dimensional models of the liquids in the bearings and inside the rotor to low-dimensional models. This enables not only transient simulations in less time, but also systematic methods, such as numerical bifurcation analysis. The expected large influence of the liquid filling on the stability has been confirmed and needs to be investigated further, for all parameters and for a wider range of their values. The current results are only first steps towards a comprehensive understanding of rotors partially filled with liquids in lubricated journal bearings and their dynamics.

REFERENCES

Berman, A., Lundgren, T. and Cheng, A. (1985). Asynchronous whirl in a rotating cylinder partially filled with liquid, *Journal of Fluid Mechanics* **150**: 311–327.

Brommundt, E. and Ostermeyer, I. G. (1986). Stabilität eines fliegend anisotrop gelagerten Rotors, der Flüssigkeit enthält, *Ingenieur-Archiv* **56**(5): 379–388.

Daich, I. and Bar, I. (1973). Vibrations of a rotating solid body containing a cavity partially filled with a viscous fluid, *Prikladnaia Mekhanika* **9**: 64–69.

Derendyaev, N., Vostrukhov, A. and Soldatov, I. (2006). Stability and Andronov-Hopf bifurcation of steady-state motion of rotor system partly filled with liquid: continuous and discrete models, *Journal of applied mechanics* **73**(4): 580–589.

Dhooge, A., Govaerts, W. and Kuznetsov, Y. A. (2003). MATCONT: a MATLAB package for numerical bifurcation analysis of odes, *ACM Transactions on Mathematical Software (TOMS)* **29**(2): 141–164.

Gasch, R., Nordmann, R. and Pfützner, H. (2006). *Rotordynamik*, Springer-Verlag.

Gümbel, L. and Everling, E. A. (1925). *Reibung und Schmierung im Maschinenbau*, Krayn.

Hendricks, S. and Morton, J. (1979). Stability of a rotor partially filled with a viscous incompressible fluid, *Journal of Applied Mechanics* **46**(4): 913–918.

Hori, Y. (1959). A theory of oil whip, *ASME J. Appl. Mech* **26**: 189–198.

Hummel, C. (1926). *Kritische Drehzahlen als Folge der Nachgiebigkeit des Schmiermittels im Lager*, Vol. 287, AW Zickfeldt.

Kollmann, F. G. (1962). Experimentelle und theoretische Untersuchungen über die kritischen Drehzahlen flüssigkeitsgefüllter Hohlkörper, *Forschung auf dem Gebiet des Ingenieurwesens A* **28**(4): 115–123.

Kuznetsov, Y. A. (2013). *Elements of applied bifurcation theory*, Vol. 112, Springer Science & Business Media.

Langthjem, M. and Nakamura, T. (2014). On the dynamics of the fluid balancer, *Journal of Fluids and Structures* **51**: 1–19.

Lichtenberg, G. (1981). *Die Schwingungen eines flüssigkeitsgefüllten Rotors unter Berücksichtigung der Kreiselwirkung*, PhD thesis.

Lund, J. W. (1966). *Self-excited, stationary whirl orbits of a journal in a sleeve bearing*, Rensselaer Polytechnic Institute.

Moiseyev, N. N. and Rumyantsev, V. (2012). *Dynamic stability of bodies containing fluid*, Vol. 6, Springer Science & Business Media.

Moser, F. (1993). *Stabilität und Verzweigungsverhalten eines nichtlinearen Rotor-Lager-Systems*, PhD thesis, TU Wien.

Newkirk, B. and Taylor, H. (1925). Shaft whipping due to oil action in journal bearings, *General Electric Review* **28**(8): 559–568.

Reynolds, O. (1886). On the theory of lubrication and its application to mr. Beauchamp Tower's experiments, including an experimental determination of the viscosity of olive oil., *Proceedings of the Royal Society of London* **40**(242-245): 191–203.

Shampine, L. F. and Reichelt, M. W. (1997). The MATLAB ode suite, *SIAM journal on scientific computing* **18**(1): 1–22.

Shaw, J. and Shaw, S. W. (1990). The effects of unbalance on oil whirl, *Nonlinear Dynamics* **1**(4): 293–311.

Sommerfeld, A. (1955). Vorlesungen über theoretische Physik.

Stodola, A. (1925). Kritische Wellenstörung infolge der Nachgiebigkeit des Oelpolsters im Lager, *Schweizerische Bauzeitung* **85**(21): 265–266.

Stokes, S. G. G. (1847). *Supplement to a memoir on some cases of fluid motion*, Printed at the Pitt Press by John W. Parker.

Szeri, A. Z. (2005). *Fluid film lubrication: theory and design*, Cambridge University Press.

Wolf, J. A. (1968). Whirl dynamics of a rotor partially filled with liquid, *Journal of Applied Mechanics* **35**(4): 676–682.